# New directions in hydrogeochemical transport modeling: Incorporating multiple kinetic and equilibrium reaction pathways

Carl I. Steefel
*Earth and Environmental Sciences Directorate, Lawrence Livermore National Laboratory, USA*

ABSTRACT: At least two distinct kinds of hydrogeochemical models have evolved historically for use in analyzing contaminant transport, but each has important limitations. One kind, focusing on organic contaminants, treats biodegradation reactions as parts of relatively simple kinetic reaction networks with no or limited coupling to aqueous and surface complexation and mineral dissolution/precipitation reactions. A second kind, evolving out of the speciation and reaction path codes, is capable of handling a comprehensive suite of multicomponent complexation (aqueous and surface) and mineral precipitation and dissolution reactions, but has not been able to treat reaction networks characterized by partial redox disequilibrium and multiple kinetic pathways. More recently, various investigators have begun to consider biodegradation reactions in the context of comprehensive equilibrium and kinetic reaction networks (e.g. Hunter et al. 1998, Mayer 1999). Here we explore two examples of multiple equilibrium and kinetic reaction pathways using the reactive transport code GIMRT98 (Steefel, in prep.): 1) a computational example involving the generation of acid mine drainage due to oxidation of pyrite, and 2) a computational/field example where the rates of chlorinated VOC degradation are linked to the rates of major redox processes occurring in organic-rich wetland sediments overlying a contaminated aerobic aquifer.

## 1 INTRODUCTION

While not yet at a stage of maturity such that they can be used routinely for predictive purposes, hydrogeochemical transport models have proven useful as interpretive tools when applied to a variety of problems in different Earth environments (see Steefel & Van Cappellen 1998 and Lichtner et al. 1996 for recent reviews). A rapid and ongoing evolution of the models has been sparked by the rapid increase in computational power available. One obvious way in which the hydrogeochemical models have evolved is through the coupling of explicit transport processes to the geochemical reaction network. This by itself is perhaps the single most important evolutionary step in hydrogeochemical modeling, but has been discussed elsewhere (see Steefel & Lasaga 1992). Another important aspect of hydrogeochemical and hydrogeochemical transport modeling has to do with the nature of the reaction network used to describe the natural system. The evolution of thinking on how to handle reaction networks in hydrogeochemical modeling is the subject of this paper.

The description of reaction networks in transport codes has historically followed two distinct lines depending on the kind of problems investigated. One important class of models are referred to loosely as “biodegradation" models. The simple forms of these models consider a single organic compound (e.g. TCE) which serves as the electron donor for what is commonly a single electron acceptor (e.g. $O_2$). The biodegradation reaction is then often described as a rate-limited process with either zeroeth or first order kinetics. As pointed out by Hunter et al. (1998), the zeroeth and first order rate approaches represent end-member formulations of Monod rate laws where a microbial population makes use of an electron donor (usually some form of organic carbon) and an electron acceptor to extract energy for their own cell growth. More sophisticated models may include terms for an explicit biomass or may include multiple electron acceptors (e.g. $O_2$ and $NO_3$) or donors (e.g. $CH_4$ and $SO_4^{-2}$). More complicated “biogeochemical" models of the kind discussed by Hunter et al. (1998) and in this paper may not necessarily use more complicated schemes for the biodegradation reactions themselves, since Monod-type formulations are still the standard approach. Rather, they differ primarily in the description of the network of biogeochemical and geochemical reactions within which the biodegradation reactions occur. By considering a more comprehensive re-

action network, it is possible to incorporate additional effects or processes which might affect the rates of biodegradation, for example, the concentration of external electron donors or acceptors. In addition, the more comprehensive reaction network allows one to consider the effects of the biodegradation reactions themselves on other key geochemical parameters like pH which can control metal co-contaminant mobility.

The other important class of hydrogeochemical models, referred to by Hunter et al. (1998) as "geochemical" models, began with the development of speciation and reaction path models (e.g. Wolery 1979, Reed 1982). The reaction path models eventually gave rise to a class of hydrogeochemical transport models which, despite having explicitly added coupled transport, used the same general treatment for the reaction network. Examples of this class of hydrogeochemical transport model are GIMRT/OS3D (Steefel & Yabusaki 1996), and early versions of HYDROGEOCHEM (Yeh and Tripathi 1991). These numerical models, like the reaction path models which came before them, were designed primarily to link aqueous and surface complexation reactions with mineral dissolution and precipitation reactions. An extensive network of complexation reactions, for example, is often necessary to describe mineral solubilities accurately as a function of master variables such as pH and $p_{O_2}$. Aqueous complexation can also have a strong effect on transport properties of reactive solutes by determining the dominant form in which the solute appears. For example, $^{60}Co$ may exist either as the free ion $Co^{+2}$ or as the complex $CoEDTA^{-}$ in EDTA-rich solutions. The speciation in this case has a direct effect on the mobility of the radionuclide, since in near-neutral pH waters the cation will adsorb to a negatively charged Fe-hydroxide while the anion $CoEDTA^{-}$ will not (Szecsody et al. 1998).

The "geochemical" approach to hydrogeochemical transport modeling, evolving as it did out of speciation/solubility and reaction path codes, is ideally suited for predominantly equilibrium problems. Many aqueous and surface complexation reactions occur sufficiently rapidly that they can be considered to be at equilibrium. As pointed out by numerous workers, the stoichiometry of equilibrium reaction networks is non-unique, that is, there are multiple ways of writing the reactions that are entirely equivalent from a mathematical point of view (Bethke 1996). Although the various reaction stoichiometries may not lead to entirely equivalent numerical behavior, the equilibrium reaction networks can be considered to be largely path-independent. Moreover, a single reaction is all that is needed to represent an equilibrium pathway, since other pathways are redundant. In the case of kinetically-controlled reactions, however, the individual pathway becomes important. One kinetic pathway need not proceed at the same rate as another pathway even though both pathways might eventually reach the same end point. In fact, multiple parallel pathways are both possible and common in low temperature systems characterized by slow reactions. Microbially-mediated oxidation-reduction (redox) reactions are the best example of these kind of kinetically-controlled reaction networks where multiple pathways exist.

Although it is often the case that the kind of geochemical or biogeochemical system considered leads naturally to one or the other of the historically distinct approaches to modeling hydrogeochemical transport, in other cases a mixed approach will be required. While the dominant redox reactions in a low temperature hydrogeochemical system may be governed primarily by slow, microbially-mediated processes, fast reactions (e.g. non-redox aqueous and surface complexation reactions) may occur as well. All of these effects can exert an important control on contaminant transport, for example. There is a need, therefore, for a new generation of hydrogeochemical transport models that incorporate both equilibrium and kinetic reaction networks.

## 2 A COMPUTATIONAL EXAMPLE INVOLVING ACID MINE DRAINAGE

We present here a computational example of a mixed equilibrium-kinetic reaction network which describes some of the major geochemical and biogeochemical processes taking place in a typical acid mine drainage setting. While no attempt is made to compare the results to an actual field example due to lack of space, the calculation is designed to be relatively realistic except in the neglect of potential pH buffering phases (carbonate and silicate minerals). We focus instead on the oxidation of pyrite via two separate pathways: oxidative dissolution by 1) molecular oxygen and 2) by ferric iron. As has been shown by a number of experimental and field workers (McKibben & Barnes 1986, Williamson & Rimstidt 1994), these are the two most important (although not the only) mechanisms by which pyrite is oxidized in near-surface environments. Acid mine drainage is primarily the result of physical and chemical processes taking place within the vadose zone, since a gas phase rich in oxygen is essential for initiating and driving the system. As an example, we consider an unsaturated zone developed within acid mine tailings with a water table at 4 meters. To keep the analysis simple, we assume steady-state flow of 1 m/yr, a porosity of 40%, and steady-state water saturation averaging 0.5 from the surface to 3.8 meters depth and a capillary fringe extending from 3.8 meters to the water table at 4 meters depth. $O_2$ and $CO_2$ gas are transported in the gas phase only via molecular diffusion. A gas diffusion coefficient of $10^{-6}$ $m^2 s^{-1}$ is assumed.

The relevant pyrite dissolution reactions are:

$$FeS_2 + 3.5\,O_2 + H_2O \rightarrow Fe^{+2} + 2\,SO_4^{-2} + 2\,H^+ \quad (1)$$

and

$$FeS_2 + 14\,Fe^{+3} + 8\,H_2O \rightarrow 15\,Fe^{+2} + 2\,SO_4^{-2} + 16\,H^+ \quad (2)$$

We use the rate laws proposed for these parallel reaction pathways by Williamson & Rimstidt (1994):

$$R_{O_2} = \left(10^{-8.10}\right) \frac{[O_2]^{0.5}}{[H^+]^{0.11}} \quad (3)$$

and

$$R_{Fe^{+3}} = \left(10^{-8.58}\right) \frac{[Fe^{+3}]^{0.3}}{[Fe^{+2}]^{0.47}[H^+]^{0.32}} \quad (4)$$

Since these reactions occur in parallel, the fastest one will dominate the overall rate.

These two dissolution pathways for pyrite are linked by the aqueous phase reaction

$$Fe^{+2} + 0.25\,O_2 + H^+ \rightarrow Fe^{+3} + 0.5\,H_2O. \quad (5)$$

Where reaction 5 is sufficiently fast that local equilibrium can be assumed, the mass action equation for reaction 5 allows reaction 1 to be written as reaction 2 (or vice versa). In this case, therefore, only a single reaction stoichiometry and equilibrium constant for pyrite dissolution is necessary and the choice of which one is used is arbitrary. In the case that $Fe^{+3}$, $Fe^{+2}$, and $O_2$ are in equilibrium, therefore, the net effect of the two dissolution pathways is to cause a change in the rate law for the overall pyrite dissolution reaction depending on whether the dominant oxidant is $Fe^{+3}$ or $O_2$.

In the case where the Fe(II)-Fe(III) redox couple and the $O_2$-$H_2O$ redox couple are not in equilibrium (i.e. reaction 5 is slow), both pyrite dissolution pathways must be retained as independent, parallel pathways. Each pyrite dissolution reaction is also associated with its own equilibrium constant and ion activity product, since equilibration with reaction 2 does not necessarily imply that reaction 1 is at equilibrium if reaction 5 ($Fe^{+2}$ oxygenation) is slow. The abiotic oxygenation of ferrous iron has been studied by Singer & Stumm (1970) and Wehrli (1990) who found it to be strongly pH-dependent and rapid at near-neutral pH values and pH-independent and slow below about pH 4. The rate laws for abiotic ferrous iron oxygenation from Wehrli (1990) are:

$$R_0 = \left(10^{-5.10}\right)[Fe^{+2}][O_2(aq)] \quad (6)$$

$$R_1 = \left(10^{1.40}\right)[Fe(OH)^+][O_2(aq)] \quad (7)$$

$$R_2 = \left(10^{6.90}\right)[Fe(OH)_2(aq)][O_2(aq)] \quad (8)$$

where in each case the second order rates constants have units of M $s^{-1}$. The formation of the hydroxy complexes increases the rate of Fe(II) oxygenation, so that the overall oxygenation rate is at a minimum at low pH. Because the Fe(II) oxygenation reaction and the oxidation of pyrite are sequential reactions, the slowest of the two will be the rate-limiting step in the overall dissolution of pyrite.

A number of workers have reported that at low pH where the abiotic Fe(II) oxygenation rate is slow, mediation by the bacteria *Thiobacillus ferrooxidans* increases the rate of reaction by up to 5 orders of magnitude (Singer & Stumm 1970, Nordstrom & Southam 1997). The microbially-mediated oxygenation of ferrous iron is treated here using a dual Monod kinetics given by

$$R = k_{max}\left(\frac{[eA]}{([eA] + K_{eA})}\right)\left(\frac{[eD]}{([eD] + K_{eD})}\right)(I_n) \quad (9)$$

where $k_{max}$ is the maximum rate of the reaction (M $s^{-1}$), $[eA]$ and $[eD]$ are the concentrations in moles per liter of the electron acceptor and donor respectively, and $K_{eA}$ and $K_{eD}$ are the half-saturation constants associated with the electron acceptor and donor respectively. $I_n$ refers to the inhibition of a particular pathway by energetically more favorable ones. The inhibition functions for any one pathway are assumed to have a hyperbolic form

$$I_n = \prod_{i=1}^{N_{in}} \frac{K_i}{(K_i + [C_i])} \quad (10)$$

where $K_i$ and $[C_i]$ refer to the inhibition constants and concentrations respectively of the $N_{in}$ species inhibiting a particular pathway. No inhibition of $Fe^{+2}$ oxygenation is included here, although inhibition functions are used in the second example discussed below. The biotic rate of $Fe^{+2}$ oxygenation occurs in parallel with the abiotic rate, so the effects are additive. For the simulations, a Monod rate constant of $5 \times 10^{-7}$ M $s^{-1}$ is assumed (Nordstrom & Southam 1997). All forms of dissolved Fe(II) are assumed to be bioavailable, so the electron donor concentration refers to total $Fe^{+2}$ rather than the concentration of the free ion $Fe^{+2}$. Half-saturation constants have not been reported, but Nordstrom & Southam (1997) indicate that the Fe(II) oxygenation rate is observed to be zeroeth-order over a wide range of ferrous iron concentrations. Accordingly, we use relatively low half-saturation constants of 1 $\mu$M for both electron acceptor and donor.

The calculations are carried out assuming infiltration of a dilute water of pH 5 in equilibrium with the atmosphere at 1 m/yr. The reactive surface area of pyrite is arbitrarily set to 0.1 $m^2$ $m^{-3}$ rock. Other

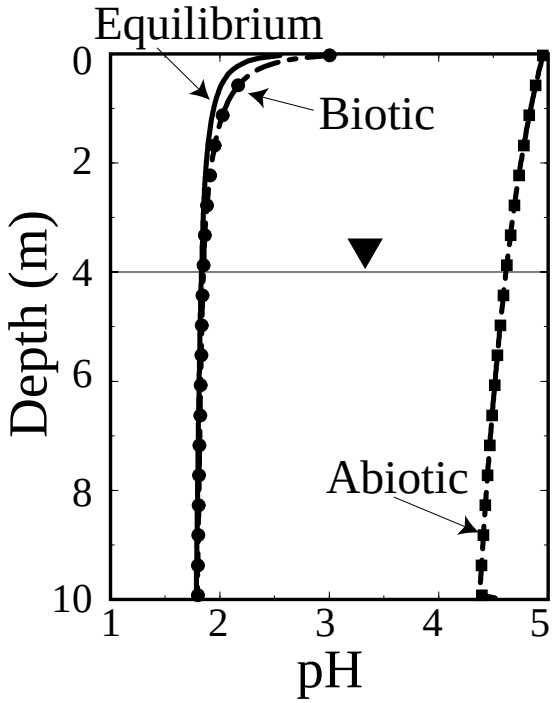


Figure 1: Calculated pH profiles as a function depth resulting from pyrite dissolution for three different cases of Fe(II) oxygenation by $O_2$.

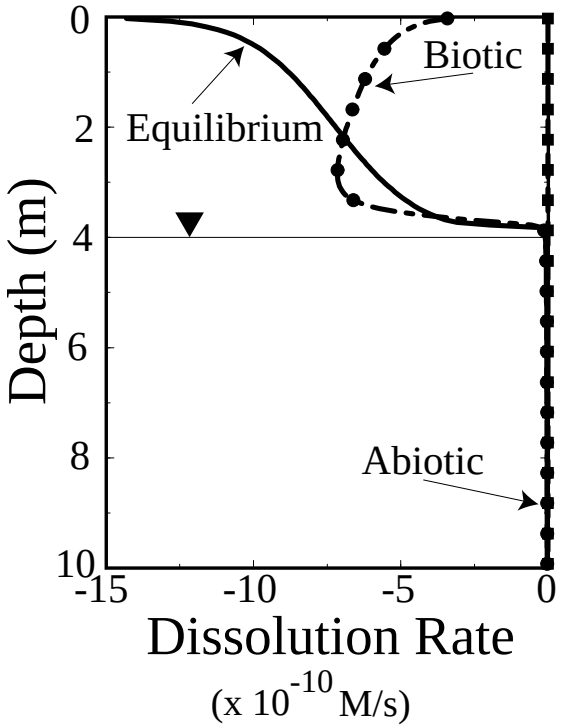


Figure 2: Calculated pyrite dissolution profiles via the ferric oxidation mechanism (reaction 2) for three different cases of Fe(II) oxygenation by $O_2$.

phases which would normally act to buffer the pH like carbonate and silicate minerals are not included in the calculation, thus producing a pH profile which only decreases with depth. In each case, the calculations are carried out using the pyrite oxidation rate laws proposed by Williamson & Rimstidt (1994), while the treatment of the Fe(II) oxygenation is varied so as to highlight the important role of this reaction in the overall reaction network. Three cases are considered: 1) aqueous Fe(II), Fe(III), and $O_2$ are in equilibrium (i.e. the traditional "geochemical" treatment of redox), 2) the Fe(II) oxygenation reaction occurs only abiotically, following the rate laws proposed by Wehrli (1990), and 3) the abiotic rate laws of Wehrli (1990) are combined with a dual Monod expression for the microbially-mediated Fe(II) oxygenation with a maximum rate given by Nordstrom & Southam (1997).

Figure 1 shows the computed pH profiles resulting from the oxidation of pyrite for the three cases under consideration. Note that the biotic case in which *Thiobacillus ferrooxidans* catalyzes the reaction nearly reproduces the equilibrium case. In this case, the rate of Fe(II) oxygenation is faster than the rate of pyrite oxidation (primarily reaction 2), so pyrite oxidation becomes the rate limiting step in the overall reaction network, in agreement with the conclusions of Nordstrom & Southam (1997). The rate profiles for the oxidation of pyrite by Fe(III), however, are not identical in the biotic and equilibrium case (Fig. 2). In the abiotic case the slow rate of Fe(II) oxygenation at low pH limits the production of Fe(III) used to oxidize the pyrite. A second oxidation pathway using molecular oxygen is available (reaction 1), but it is much slower than the oxidation by ferric iron, so the overall rate of pyrite is slowed significantly relative to the biotic or equilibrium case. This is obvious in both the pH profile (Fig. 1) and in the plot of the rate of the pyrite oxidation by ferric iron pathway (Fig. 2) which is essentially zero. The fact that the abiotic Fe(II) oxygenation mechanism does not result in the low pH values typically observed in actual acid mine drainage sites can be used as an argument for the important role of *Thiobacillus ferrooxidans* in controlling geochemical processes in acid mine environments.

## 3 A FIELD/COMPUTATIONAL EXAMPLE INVOLVING VOC DEGRADATION

A second example illustrates more directly how biodegradation problems can be viewed within the context of a larger reaction network. The example involves chlorinated volatile organic carbon (VOC) degradation at the Aberdeen Proving Ground in Maryland, USA, as discussed by Lorah & Olsen (1999). Release of waste products in the past has resulted in contamination of a 12-14 m thick shallow sand aquifer which is overlain locally by wetland sediments. The wetland sediments are 1.8 to 3.6 m thick and consist of a lower silty unit and an upper peat unit. Groundwater flow in the wetland area is predominantly upwards, with an average linear flow velocity of 0.6 m $yr^{-1}$ estimated by Lorah & Olsen (1999). The aquifer below the wetland sediments is dominated by aerobic con-

ditions, but is highly contaminated with chlorinated volatile organic compounds (VOCs), the most important of which are PCA (1,1,2,2-tetrachloroethane) and TCE (trichloroethylene). In contrast, anaerobic conditions occur in the organic carbon-rich wetland sediments, where well-defined, discrete zones of dissimilatory iron reduction, sulfate reduction, and methanogenesis are apparent.

There is clear field evidence of the natural attenuation of the chlorinated VOCs within the anaerobic wetland sediments (Lorah & Olsen 1999). Various workers have reported that chlorinated VOCs can be anaerobically degraded under a variety of reducing conditions, including nitrate reduction, dissimilatory iron reduction, sulfate reduction, and methanogenesis (Lorah & Olsen 1999). Based on laboratory studies, the rate of biodegradation appears to be greatest under methanogenic conditions (Lorah & Olsen 1999).

The excellent field study by Lorah & Olsen (1999) provides us with an opportunity to study the biodegradation of a suite of chlorinated VOCs in the context of the major redox processes occurring in organic-rich sediment. A reactive transport modeling analysis can be used to determine field biodegradation rates and to correlate these with in situ rates of the primary redox processes like sulfate reduction and methanogenesis. For the sake of brevity, we restrict ourselves here to a one-dimensional analysis of steady-state flow and transport up through the wetland sediments, attempting to match the water quality profiles given by Lorah & Olsen (1999) for piezometer WB-26.

Redox processes at the Aberdeen proving ground are dominated by the heterotrophic oxidation of organic carbon which is abundant in the sediments overlying the aquifer (Lorah & Olsen 1999). In piezometer WB-26, for example, the aerobic conditions within the aquifer give way upward along a flow path to discrete zones of dissimilatory Fe reduction, sulfate reduction, and methanogenesis. These reactions are modelled under the assumption that organic carbon is present well in excess of its limiting concentration (half-saturation constant) above 4.8 meters depth, while the electron acceptor effect on the reaction rate is treated with a standard Monod expression (Eqn. 9). In keeping with the steady-state assumption, the effect of the biomass is incorporated into the rate constant rather than being treated explicitly as a time-dependent term (Hunter et al. 1998). Kinetic reactions and associated rate and half-saturation constants used in the simulations are given in Table 1. Inhibition of organic carbon oxidation pathways by energetically more favored pathways is assumed to occur. Inhibition constants are taken as the half-saturation constants of the electron acceptor for the more favorable pathway (e.g. $O_2$ in the case of dissimilatory Fe reduction, sulfate reduction, and methanogenesis and Fe-hydroxide in the case of sulfate reduction and methanogenesis). In this way, the sequence of most to least energetically favored organic carbon oxidation pathways observed in the field (aerobic respiration, followed in order by dissimilatory Fe reduction, sulfate reduction, and methanogenesis) can be duplicated with the simulations (Hunter et al. 1998). Equilibrium complexation reactions (e.g. the formation of the hydroxy complexes of $Fe^{+2}$ and $Fe^{+3}$) are also included in the simulations. Accordingly, the half-saturation constants in Table 1 refer to total concentrations. Amorphous iron sulfide is allowed to precipitate via both direct reaction of amorphous Fe-hydroxide with dissolved sulfide and by reaction of aqueous Fe(II) and dissolved sulfide (Table 1). Adsorption of the VOCs on to organic carbon, which in transient cases could be an important effect, is neglected in the simulations.

For the degradation of the chlorinated VOCs, we consider a simplified version of the reaction network presented by Lorah & Olsen (1999) (Fig. 3). The vertical arrows refer to hydrogenolysis pathways, sequential reductive dechlorination reactions involving the transfer of two electrons (Lorah & Olsen 1999). The angled arrow from PCA to DCE is another reductive dechlorination reaction involving the transfer of two electrons and is referred to as dichloroelimination. Other pathways have been recognized, including an abiotic transformation of PCA to TCE (dehydrochlorination) and a dichlorelimination transformation of TCA to vinyl chloride, but are neglected here. All of the VOC degradation reactions involve the transfer of two electrons, but a number of different electron donors are possible. The importance of Fe(II) as an electron donor is demonstrated by the field study of Lorah & Olsen (1999) who show substantial degradation of both PCA and TCE in the presence of dissolved Fe(II) and in the absence of significant sulfate reduction and methanogenesis. Accordingly, for each of the pathways shown in Figure 3, we consider the possibility of reduction by dissolved Fe(II), sulfide, and methane. Each reduc-

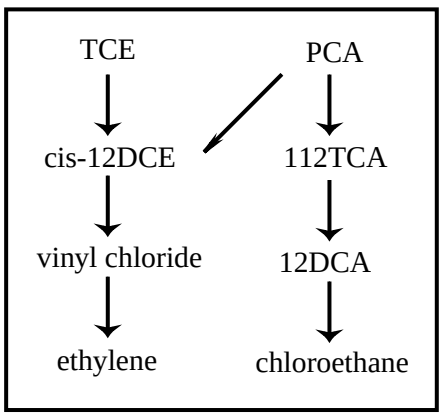


Figure 3: Reaction network (simplified after Lorah & Olsen 1999) used in the simulations of chlorinated volatile organic compounds in this paper.

Table 1: Reaction pathways and associated rate and half-saturation constants used in simulations.

| Reaction | Rate ($Ms^{-1}$) | $K_{eA}$ ($\mu$M) | $K_{eD}$ ($\mu$M) |
|---|---|---|---|
| Organic carbon oxidation | | | |
| $CH_2O + O_2 \rightarrow CO_2 + H_2O$ | $3 \times 10^{-6}$ | 20 | 0 |
| $CH_2O + 4\ Fe(OH)_3(am) + 2\ H^+ \rightarrow CO_2 + 4\ Fe^{+2} + \frac{11}{4}\ H_2O$ | $1 \times 10^{-6}$ | 60 | 0 |
| $CH_2O + \frac{1}{2}\ SO_4^{-2} + \frac{1}{2}\ H^+ \rightarrow CO_2 + \frac{1}{2}\ HS^- + H_2O$ | $3 \times 10^{-5}$ | 30 | 0 |
| $CH_2O \rightarrow \frac{1}{2}\ CO_2 + \frac{1}{2}\ CH_4$ | $3 \times 10^{-5}$ | 0 | 0 |
| VOC degradation | | | |
| $TCE + 2\ Fe^{+2} + H^+ \rightarrow DCE + 2\ Fe^{+3} + Cl^-$ | $2 \times 10^{-5}$ | 100 | 10 |
| $TCE + \frac{1}{4}\ HS^- + H_2O \rightarrow DCE + \frac{1}{4}\ SO_4^{-2} + Cl^-$ | $1 \times 10^{-4}$ | 100 | 1 |
| $TCE + \frac{1}{4}\ CH_4 + \frac{1}{2}\ H_2O \rightarrow DCE + \frac{1}{4}\ CO_2 + Cl^-$ | $1 \times 10^{-4}$ | 100 | 10 |
| $PCA + 2\ Fe^{+2} + H^+ \rightarrow DCE + 2\ Fe^{+3} + Cl^-$ | $2 \times 10^{-5}$ | 100 | 1 |
| $PCA + \frac{1}{4}\ HS^- + H_2O \rightarrow DCE + \frac{1}{4}\ SO_4^{-2} + Cl^-$ | $2 \times 10^{-4}$ | 100 | 1 |
| $PCA + \frac{1}{4}\ CH_4 + \frac{1}{2}\ H_2O \rightarrow DCE + \frac{1}{4}\ CO_2 + Cl^-$ | $1 \times 10^{-3}$ | 100 | 10 |
| $DCE + 2\ Fe^{+2} + H^+ \rightarrow VC + 2\ Fe^{+3} + Cl^-$ | $1 \times 10^{-4}$ | 100 | 10 |
| $DCE + \frac{1}{4}\ HS^- + H_2O \rightarrow VC + \frac{1}{4}\ SO_4^{-2} + Cl^-$ | $2 \times 10^{-4}$ | 100 | 1 |
| $DCE + \frac{1}{4}\ CH_4 + \frac{1}{2}\ H_2O \rightarrow VC + \frac{1}{4}\ CO_2 + Cl^-$ | $2 \times 10^{-4}$ | 100 | 50 |
| $VC + 2\ Fe^{+2} + H^+ \rightarrow C_2H_4 + 2\ Fe^{+3} + Cl^-$ | $1 \times 10^{-3}$ | 100 | 10 |
| $VC + \frac{1}{4}\ HS^- + H_2O \rightarrow C_2H_4 + \frac{1}{4}\ SO_4^{-2} + Cl^-$ | $1 \times 10^{-3}$ | 100 | 1 |
| $VC + \frac{1}{4}\ CH_4 + \frac{1}{2}\ H_2O \rightarrow C_2H_4 + \frac{1}{4}\ CO_2 + Cl^-$ | $5 \times 10^{-4}$ | 100 | 10 |
| $PCA + 2\ Fe^{+2} + H^+ \rightarrow TCA + 2\ Fe^{+3} + Cl^-$ | $1 \times 10^{-4}$ | 100 | 10 |
| $PCA + \frac{1}{4}\ HS^- + H_2O \rightarrow TCA + \frac{1}{4}\ SO_4^{-2} + Cl^-$ | $1 \times 10^{-4}$ | 100 | 1 |
| $PCA + \frac{1}{4}\ CH_4 + \frac{1}{2}\ H_2O \rightarrow TCA + \frac{1}{4}\ CO_2 + Cl^-$ | $1 \times 10^{-4}$ | 100 | 10 |
| $TCA + 2\ Fe^{+2} + H^+ \rightarrow DCA + 2\ Fe^{+3} + Cl^-$ | $2.5 \times 10^{-4}$ | 100 | 10 |
| $TCA + \frac{1}{4}\ HS^- + H_2O \rightarrow DCA + \frac{1}{4}\ SO_4^{-2} + Cl^-$ | $2.5 \times 10^{-4}$ | 100 | 1 |
| $TCA + \frac{1}{4}\ CH_4 + \frac{1}{2}\ H_2O \rightarrow DCA + \frac{1}{4}\ CO_2 + Cl^-$ | $2.5 \times 10^{-4}$ | 100 | 10 |
| $DCA + 2\ Fe^{+2} + H^+ \rightarrow C_2H_5Cl + 2\ Fe^{+3} + Cl^-$ | $5 \times 10^{-5}$ | 100 | 10 |
| $DCA + \frac{1}{4}\ HS^- + H_2O \rightarrow C_2H_5Cl + \frac{1}{4}\ SO_4^{-2} + Cl^-$ | $1 \times 10^{-4}$ | 100 | 1 |
| $DCA + \frac{1}{4}\ CH_4 + \frac{1}{2}\ H_2O \rightarrow C_2H_5Cl + \frac{1}{4}\ CO_2 + Cl^-$ | $1 \times 10^{-4}$ | 100 | 10 |
| Secondary redox | | | |
| $Fe(OH)_3(am) + \frac{1}{2}\ H_2S + 2\ H^+ \rightarrow Fe^{+2} + \frac{1}{2}\ S^0 + 3\ H_2O$ | $6.3 \times 10^{-6}$ | | |
| Non-redox precipitation-dissolution | | | |
| $FeS(am) + H^+ \rightarrow Fe^{+2} + HS^-$ | $1 \times 10^{-6}$ | | |

tion reaction is written with a dual Monod formulation (Eqn. 9), with the rate and half-saturation constants for both electron donor and acceptor given in Table 1. No inhibition terms were included for the VOC degradation reactions.

Figure 4-A show the concentrations of $O_2$ and $SO_4^{-2}$ measured in porewater from piezometer WB-26 (Lorah & Olsen 1999) along with the profiles (solid lines) computed by GIMRT98 (Steefel, in prep.). The porewater data from piezometer WB-26 indicates a zone about 1.8 meters thick in which aerobic respiration and dissimilatory Fe reduction occur without substantial sulfate reduction (between sample points at 4.6 and 2.8 meters depth). Although sulfate concentrations are not high, the data also show a discrete sulfate reduction zone between 2.8 meters and about 1.2 meters depth. Concentrations of the reduced species $Fe^{+2}$, $HS^-$, and $CH_4$ are shown in Figure 4-B. The computed Fe(II) concentration shows a peak at a depth of 2.8 meters, in agreement with the data. Both computed and observed sulfide concentrations remain relatively low throughout the profile due to the precipitation of FeS. Once dissimilatory Fe reduction and sulfate reduction drop off along the flow path (i.e. with decreasing depth), methanogenesis results in high methane concentrations above about 1.2 meters.

As noted above, biodegradation of the chlorinated volatile organic compounds is linked in the simulations presented here to the concentrations of the specific electron donors rather than being treated as first order or pseudo-first order expressions. A good fit of the observed data is achieved with the GIMRT98 simulations, although the fit is non-unique because of the large number of parameters involved. Nontheless, the simulations, in conjunction with the original data, suggest some preliminary observations about the relative rates of the degradation reactions in the various anaerobic zones. In Figure 5-A, for example, the bulk of the PCA degradation occurs in the dissimilatory Fe reduction zone (compare Figure 4-B). TCE also degrades at a substantial rate within this interval as well, even though the data in Figure 4-A indicate that sulfate reduction and methanogenesis are not occurring at significant rates within this depth interval. There

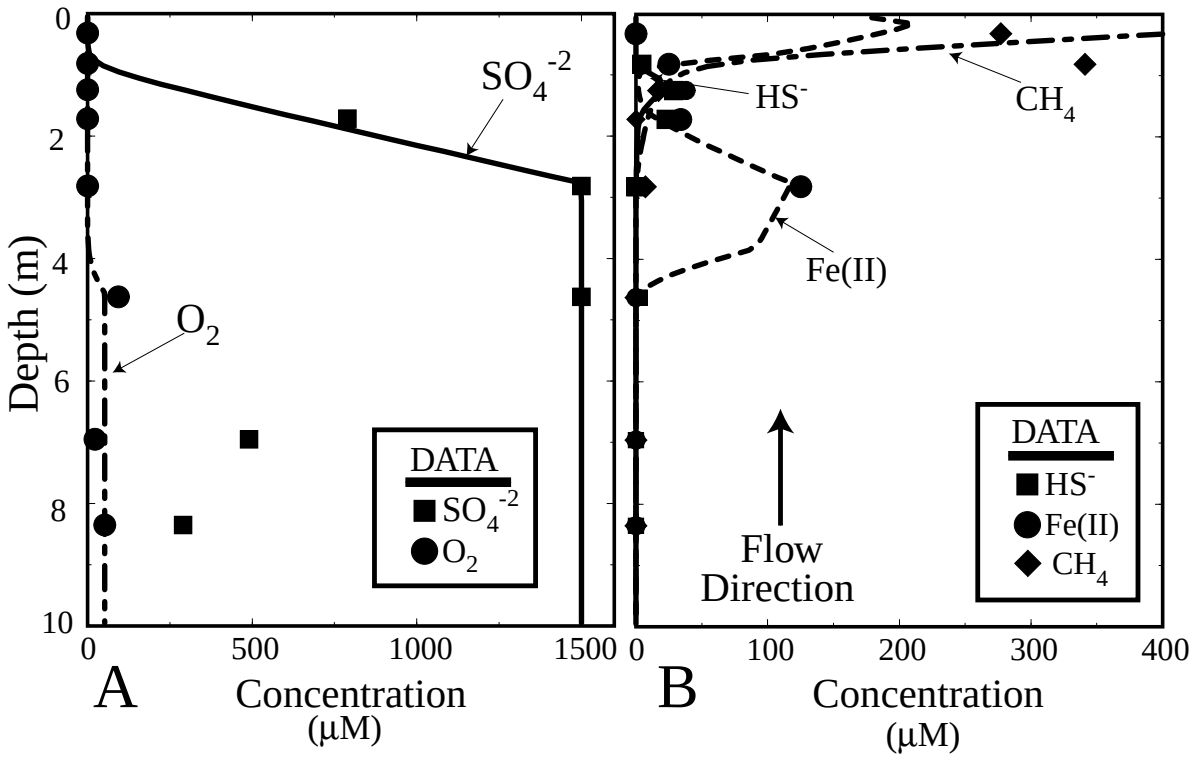


Figure 4: A: Distribution of the electron acceptors $O_2$ and $SO_4^{-2}$ as a function of depth, with data (from Lorah & Olsen 1999) shown as symbols and model results using GIMRT98 shown as lines.
B: Distribution of major electron donors $Fe^{+2}$, $HS^-$, and $CH_4$

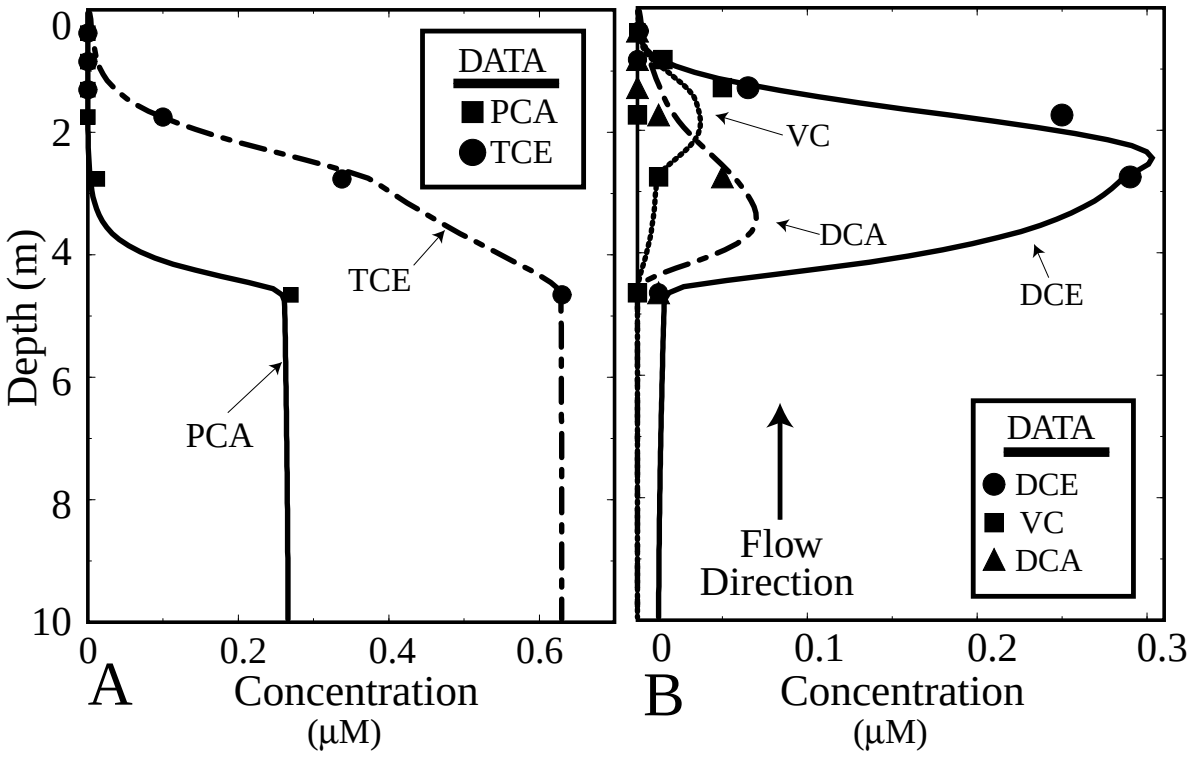


Figure 5: A: Distribution of chlorinated volatile organic carbon parents PCA and TCE. Data (from Lorah & Olsen 1999) shown as symbols and model results using GIMRT98 shown as lines.
B: Distribution of chlorinated volatile organic carbon parents DCE, VC (vinyl chloride) and DCA (TCA not shown).

is some suggestion that the rate of TCE degradation is slightly faster in the sulfate reduction zone than in the dissimilatory Fe reduction zone, but considerably more data is needed to substantiate this conclusion. Figure 5-B shows the observed and computed concentrations of the VOC daughters. In order to match the DCE data, the degradation rates in the methanogenic zone needed to be higher than the rates in the sulfate reduction and dissimilatory Fe reduction zones by factors of 5 and 50 respectively. Matching the DCA data, however, required that the rates of degradation in the sulfate reduction and methanogenic zones be only a factor of 2 higher than the rate in the dissimilatory Fe reduction zone.

## 4 CONCLUSIONS

Many groundwater and surface water systems are characterized by biogeochemical reaction networks consisting of multiple kinetic and equilibrium pathways. Two examples of such reaction networks were explored with the reactive transport code GIMRT98 (Steefel, in prep.), although the general capability for treating such reaction networks can be found in a small number of other codes developed recently, for example, PHREEQC (Parkhurst 1995) and MIN3P (Mayer 1999). The first example examined the reaction network associated with pyrite oxidation. Using the setting of acid mine drainage developed within the vadose zone, the overall rate of pyrite is shown to be limited by the rate of oxidation of pyrite by ferric iron in the case where the bacteria *Thiobacillus ferrooxidans* enhances the rate of $Fe^{+2}$ oxygenation to the point where the aqueous Fe(II)/Fe(III) redox couple is close to equilibrium. In contrast, the overall rate of pyrite oxidation is limited by the rate of $Fe^{+2}$ oxygenation when strictly abiotic conditions prevail, although these conditions do not appear to be common in nature. In a second problem involving the natural attenuation of chlorinated VOCs, it was shown that a reaction network which explicitly couples the degradation rates of the chlorinated VOCs to the concentrations of the spatially-distributed major electron donors (Fe(II), $HS^-$, and $CH_4$) could be used to match field data presented by Lorah & Olsen (1999).

## REFERENCES


Bethke, C.M. 1996. *Geochemical reaction modeling*. Oxford Univ. Press, New York, 397 p.

Hunter, K.S., Y. Wang & P. Van Cappellen 1998. Kinetic modeling of microbially-driven redox chemistry of subsurface environments: couping transport, microbial metabolism and geochemistry. *J. Hydrol.* 209: 53-80.

Lichtner, P.C., C.I. Steefel & E.H. Oelkers (ed.) 1996, *Reactive transport in porous media*. Rev. in Mineralogy 34: 438 p.

Lorah M.M. & L.D. Olsen 1999. Natural attenuation of chlorinated volatile organic compounds in a freshwater tidal wetland: Field evidence of anaerobic biodegradation. *Water Resources Res.* 34: 3811-3827.

Mayer, K.U. 1999. A numerical model for multicomponent reactive transport in variably saturated porous media. Unpubl. Ph.D. thesis, U. Waterloo, 286 p.

McKibben, M.A., & H.L. Barnes 1986. Oxidation of pyrite in low temperature acidic solutions: Rate laws and surface textures. *Geochim. Cosmochim. Acta* 50: 1509-1520.

Nordstrom, D.K. & G. Southam 1997. Geomicrobiology of sulfide mineral oxidation. In J.F. Banfield & K.H. Nealson (eds.) *Geomicrobiology: Interactions between microbes and minerals* Reviews in Mineralogy 35: 361-390.

Parkhurst, D.L. 1995, User's guide to PHREEQC—a computer program for speciation, reaction-path, advective-transport, and inverse geochemical calculations. USGS Wat. Res. Investigations Report 95-4227.

Reed, M.H. 1982. Calculation of multicomponent chemical equilibria and reaction processes in systems involving minerals, gases, and an aqueous phase. *Geochim. Cosmochim. Acta* 46: 513-528.

Singer, P.C. & W. Stumm 1970. Acid mine drainage: the rate-determining step. *Science* 167: 1121-1123.

Steefel C.I. & Lasaga A.C. 1992. Putting transport into water–rock interaction models. *Geology* 20, 680-684.

Steefel, C.I. & P. Van Cappellen 1998. Reactive transport modeling of natural systems. *J. Hydrol.* 209: 1-7.

Steefel, C.I. & S.B. Yabusaki 1996. OS3D/GIMRT, Software for Multicomponent- Multidimensional Reactive Transport, User Manual and Programmer's Guide, PNL-11166, Pacific Northwest National Laboratory, Richland, Washington.

Szecsody, J.E., J.M. Zachara, A. Chilakapati, P.M. Jardine & A.S. Ferrency 1998. Importance of flow and particle-scale heterogenetiy on $CO^{II/III}$EDTA reactive transport. *J. Hydrol.* 209: 112-136.

Wehrli, B. 1990. Redox reactions of metal ions at mineral surfaces. In W. Stumm (ed.) *Aquatic chemical kinetics. Reaction rates of processes in natural waters*. Wiley-Interscience.

Williamson, M.A. & J.D. Rimstidt 1994. The kinetics and electrochemical rate-determining step of aqueous pyrite oxidation. *Geochim. Cosmochim. Acta* 58: 5443-5454.

Wolery, T.J. 1979. Calculation of chemical equilibrium between aqueous solution and minerals: the EQ3/6 software package. Lawrence Livermore Lab. URCL-52658.

Yeh, G.T. & V.S. Tripathi 1991. A model for simulating transport of reactive multispecies components: Model development and demonstration. *Water Resources Res.* 27: 3075-3094.